ADVANCED ENGINEERING MATERIALS
www.aem-journal.com

Numerical and Experimental Evaluation of Structured Material for Use in Multiscale Topology Optimization

Ondřej Vaverka, Ondřej Červinek, Jan Jaroš, Daniel Koutný, and Libor Pantělejev*

Multiscale topology optimization is a powerful tool for engineers seeking a design with minimum weight and maximum stiffness, using a structured material in the form of a lattice structure. Furthermore, the current trend is to combine multiple lattice topologies in one component to achieve the best possible response to local loading conditions while minimizing weight. Therefore, herein, a numerical and experimental evaluation by compression tests in two directions is performed for six basic lattice topologies and two hypotheses are tested. The first hypothesis states that an additional weight saving of more than 30% can be achieved by a better choice of lattice topology. The second hypothesis is based on the manufacturing limitations of the laser powder bed fusion technology and the assumption that a favorable loading direction parallel to the building direction exists. The first hypothesis is only confirmed for loading in the direction parallel to the building direction and the second only for two lattice topologies. When both hypotheses are combined, the additional weight reduction of the multiscale topology optimization result is 44.5% according to the numerical results and 32.7% according to the experimental verification.

1. Introduction

Topology optimization as a tool to determine the optimal design of components has now been used for a long time, and since the beginning, the material used for the design has been porous.[1] Such topology optimization that separates the scales and optimizes not only the macroshape but also the structure of the material is called a multiscale topology optimization.[2] Methods using structured material were unfortunately purely theoretical at first due to the purely theoretical at first due to the computational difficulties and moreover due to the lack of manufacturing capabilities.[3] With the advent of additive manufacturing in its polymer and, more recently, metal versions, researchers working on multiscale topology optimization have finally been given a tool to realize their designs.[4] However, in order to use structured materials in multiscale topology optimization, it is important to be able to predict their mechanical properties. According to the Gibson–Ashby cellular material theory, the mechanical properties of porous materials depend on the parent material, the relative density, and the geometry of the unit cell.[5]

An aluminum alloy AlSi10Mg was chosen as the parent material for this study, as it is one of the most used materials in laser powder bed fusion (LPBF) technology. Its high stiffness to weight ratio, high thermal conductivity, and stable manufacturing process make AlSi10Mg an ideal candidate for engineering applications in many industries such as automotive or aerospace.[6,7] Furthermore, researchers agree that elastic properties of AlSi10Mg are not affected by different build orientation,[8,9] which is an important advantage for industrial use. They also agree that the only anisotropic behavior can be observed in elongation at break. However, most engineering components are predominantly operated in the elastic region and therefore this anisotropy is not considered an important disadvantage.

Due to the precipitation hardening potential of this alloy and the possibility of adjusting the resulting mechanical properties, extensive research has also been carried out in the field of postprocessing heat treatment.[10–13] Heat treatment for AlSi10Mg can be divided into two groups—annealing to relieve residual stresses and solution annealing followed by precipitation hardening, also known as T6 treatment. Mertens et al. compared these two groups and found that annealing reduces the yield strength, ultimate strength, and hardness, but increases the elongation at break.[12] On the other hand, solution treatment increases the yield strength and improves the ductility even more than annealing. The comparison was also made by Vaverka et al. who also pointed out the effect on residual stress and the induction of inner compressive stress by water cooling.[14] T6 heat treatment is used to improve the mechanical properties not only of the bulk material but also of the lattice structures. For example, Megahed et al. investigated different temperatures and holding times.[15] However, other authors used the T6 treatment as a common method for postprocessing the lattice samples, for example, Maskery et al. or Wang et al.[16,17]

O. Vaverka, O. Červinek, J. Jaroš, D. Koutný
Institute of Machine and Industrial Design
BUT Brno
Technická 2896/2, Brno 616 69, Czech Republic
E-mail: Ondrej.Vaverka@vut.cz

L. Pantělejev
Institute of Materials Science and Engineering
BUT Brno
Technická 2896/2, Brno 616 69, Czech Republic

The ORCID identification number(s) for the author(s) of this article can be found under https://doi.org/10.1002/adem.202400127.

DOI: 10.1002/adem.202400127

The mechanical properties of lattice structures made of AlSi10Mg were investigated in detail. The effect of process parameters was investigated by Fiocchi et al. or Ossola et al. and even special hatching strategies for lattice structures were proposed by Sos et al. or Vrána et al.[18–21] In the mentioned studies, the main focus is on compressive properties such as compressive strength, energy absorption, or impact energy. Other test methods such as tensile, shear, or torsion tests have also been investigated, but are less common.[22] Some researchers also compared different lattice structures to find the best one for the abovementioned properties.[23,24] Different relative densities, different cell sizes, or strut diameters have also been tested.[25,26]

However, for multiscale topology optimization, which mostly works in the elastic domain, the stiffness of the lattice structure is the most important property. This property, which is defined by the Young's modulus of elasticity (for bulk material) or the effective modulus of elasticity (for the structure), is usually not the objective of the studies. Researchers assume that the Young's modulus of elasticity remains constant with little change during heat treatment, or they use the conventional tensile specimens to predict the properties of lattice structures.[18,22,27] However, lattice structures are usually characterized by much smaller dimensions, i.e., by the wall thickness if it is a plane-based structure or by the strut diameter if it is a truss-based structure. The latter mentioned structures have been studied by Dong et al. who have shown that the Young's modulus of elasticity varies significantly with the strut diameter or build orientation of the struts.[28,29]

As horizontal geometries are not recommended due to the need for supports,[30] low mechanical properties,[29] or poor geometric accuracy,[19] the simplest truss-based lattice structures are geometrically anisotropic (see Figure 2 in Section 2.1). Despite this fact, the lattice structures in different orientations are only studied for other materials prone to material anisotropy, such as 316 L stainless steel,[31] maraging steel,[32] and titanium alloy Ti_6Al_4V,[33] or only with the means of finite element analyses.[34] Therefore, there is an urgent need for such a comparison for the most commonly used aluminum alloy, as multiscale topology optimization could significantly profit from such insights.

The acquisition of material interpolation schemes in multiscale topology optimization is nowadays often replaced by machine learning,[35,36] which is mainly used for the prediction of mechanical properties in topology optimization. These algorithms can also benefit from some complex numerical and experimental evaluations, as they can serve as input data for the learning process.

Another current trend in multiscale topology optimization (in the last 5 years) is to combine multiple lattice topologies in one component.[37–39] The main advantage of such an approach is the possibility to achieve the best possible mechanical response to local loading conditions by changing not only the relative density but also the lattice topology (see comparison in **Figure 1**). However, this method also has its problems, including the connectivity of the adjacent lattice topologies, which is the same problem as with other multiscale topology optimization approaches.[40–42] One of the possible solutions is to define lattice topologies before optimization that ensure the connectivity through a common design feature. Such lattice topologies are, e.g., basic truss-based lattice structures, in which the material is always present in all eight corners of the cube.

The purpose of multilattice methods is to propose the lightest possible lattice topology for local loading conditions. Therefore, by choosing the lattice topology, the mass saving achieved by multiscale topology optimization could be pushed even further. In the study by Aremu et al. the authors state that the face-centered cube with additional struts in the *Z*-direction (FCCZ) can withstand twice the load force at the same relative density as the body-centered cube (BCC).[34] Conversely, the FCCZ lattice topology could have a lower relative density at the same load force. As the relationship between stiffness and relative density is exponential,[43] the weight reduction can be about 30%. Hanzl et al. and Smith et al. also pointed out the importance of struts with their axis parallel to the loading direction.[32,44]

Based on the literature review, two working hypotheses were established, which are tested in this article: 1) The result of multiscale topology optimization can be improved by changing the lattice topology and maintaining the stiffness by an additional 30% weight reduction; and 2) The loading of lattice structures in the direction parallel to the build direction is always advantageous as there are no struts parallel to the build plate. Therefore, changing the manufacturing orientation of the part will save additional mass while maintaining stiffness.

From the literature review, it is clear that the combination of lattice topologies is a current trend, but the connectivity of the topologies must be ensured, and the elastic properties of aluminum lattice structures have not been studied in different directions. Therefore, the aim of this article is to compare numerically and experimentally the elastic properties of aluminum

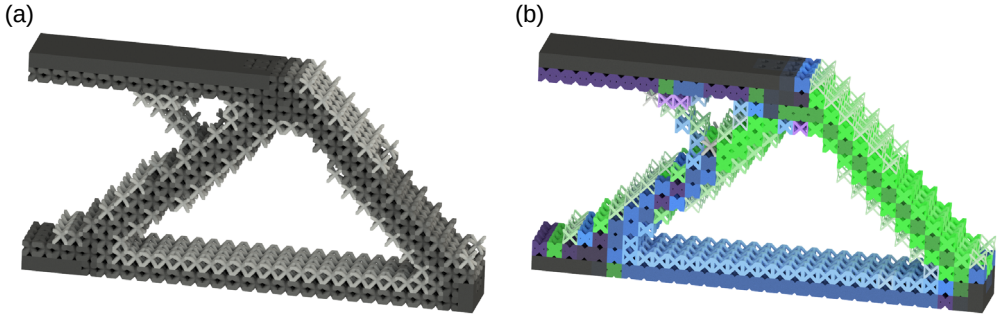

Figure 1. Results of multiscale topology optimization: a) functionally graded lattice structure and b) multilattice design—each color is different lattice topology.

truss-based lattice structures, which have a great potential for the multilattice multiscale topology optimization. Section 2 introduces the investigation methods used and Section 3 presents the results and discussion. Section 3.1 shows the results of the numerical simulations with the nominal material model (described in Section 2.5.1) and a numerical comparison of the lattice topologies in two directions. Section 3.2 is dedicated to the experimental results. As the results differ from those of the numerical simulation, Section 3.3 contains the results of the numerical simulations with a parametric material model (described in Section 2.5.1). The observed anisotropy is discussed in Section 3.4 and in Section 3.5 the lattice topologies are experimentally compared in the same way as in Section 3.1. Finally, based on the obtained results, an improved material model for material interpolation in multiscale topology optimization is proposed and experimentally verified in Section 3.6.

2. Experimental Section

2.1. Geometry of Lattice Specimens

In this study, the lattice topologies BCC, FCC, and body- and face-centered cube (BFCC) as well as their variants with additional struts in the *Z*-direction—BCCZ, FCCZ, and BFCCZ—were investigated (see **Figure 2**). These lattice topologies were selected because they satisfy two essential conditions for use in multilattice multiscale topology optimization—manufacturability (no vertical geometry) and connectivity (all struts start in the corners of the cube). All lattice specimens were 30 mm cubes consisting of 27 cells with a cell size of 10 mm. The specimens were designed with relative densities of 0.3, 0.4, 0.55, and 0.7. Therefore, each lattice cube had a different strut diameter as shown in **Table 1**.

Each specimen was fabricated twice—once for testing in the *Z*-direction and once for testing in the *XY*-direction. The reason for this is the limited area of a build platform (and the wide range of geometries tested—48 specimens in total) and an effort to minimize differences between specimens caused by fabrication or postprocessing by processing them all at once.

2.2. Production of Specimens

All specimens were fabricated from an AlSi10Mg alloy with an SLM 280^{HL} machine (SLM Solutions, Lübeck, Germany) using LPBF technology. The respective cross sections were produced with a 400 W YLR fiber laser with a spot diameter of 82 µm.

The standard process parameters specified by the manufacturer SLM Solutions were used for the build job, i.e., a laser power of 350 W, a scan speed of 930 mm s^{-1}, a hatch distance of 0.17 µm, a layer thickness of 50 µm, a preheating of the build platform of 150 °C, and a nitrogen atmosphere with an oxygen concentration below 0.5%. The scanning strategy was standard with one contour and hatch with meander scanning.

According to a previous study, the best combination of mechanical properties was observed with the T6 treatment condition, i.e., solution annealing at 520 °C for 6 h, followed by water cooling and artificial aging at 175 °C for 4 h.[14] The T6 treatment was also applied to unify the microstructure of the lattice specimens and eliminate the anisotropy of the material caused by the nonuniform heat dissipation during fabrication.[45,46]

Table 1. Specimen types with respective strut diameters.

Specimen	Strut diameter [mm]	Specimen	Strut diameter [mm]	Specimen	Strut diameter [mm]
BCC-0.3	2.70	FCC-0.3	3.04	BFCC-0.3	2.03
BCC-0.4	3.22	FCC-0.4	3.64	BFCC-0.4	2.43
BCC-0.55	3.97	FCC-0.55	4.54	BFCC-0.55	3.02
BCC-0.7	4.74	FCC-0.7	5.55	BFCC-0.7	3.67
BCCZ-0.3	2.54	FCCZ-0.3	2.86	BFCCZ-0.3	1.95
BCCZ-0.4	3.03	FCCZ-0.4	3.46	BFCCZ-0.4	2.34
BCCZ-0.55	3.74	FCCZ-0.55	4.41	BFCCZ-0.55	2.91
BCCZ-0.7	4.50	FCCZ-0.7	5.51	BFCCZ-0.7	3.53

2.3. Testing and Examination of Specimens

The mechanical tests were performed on the Zwick Z250 universal testing machine (Zwick GmbH & Co. KG, Ulm, Germany) with a load cell of 150 kN. All specimens were tested in compression with a preload of 20 N and a test speed of 1 mm min^{-1}.

From the force range F in the elastic region, the theoretical stress σ_{teor} in the specimens was calculated by dividing it by the total area of the respective cube A (≈900 mm^2 based on the actual area of the respective specimens) (Equation (1)). The force range used is represented in Equation (1) by F_1 and F_2, which stand for the force value at the beginning and end of the elastic region, respectively. The real displacement h in the selected force range F was divided by the initial height at the beginning of the interval h_1 and the strain value ε was determined (Equation (2)). The effective modulus of elasticity (EM) of the lattice specimens was calculated from the stress–strain ratio (Equation (3))

$$\sigma_{teor} = \frac{F_2 - F_1}{A} \tag{1}$$

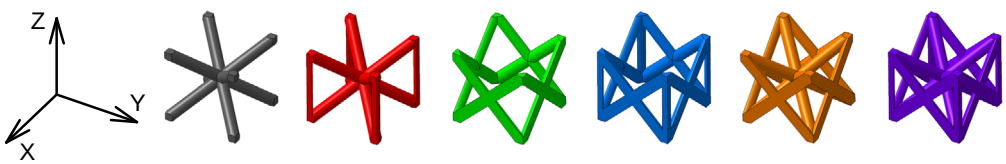

Figure 2. Topologies of lattice cells (from left to right: BCC, BCCZ, FCC, FCCZ, BFCC, and BFCCZ).

$$\varepsilon = \frac{h}{h_1} = \frac{h_2 - h_1}{h_1} \tag{2}$$

$$EM = \frac{\sigma_{\text{teor}}}{\varepsilon} \tag{3}$$

Two fundamental properties were calculated from all experiments and simulations. The first property was the effective modulus of elasticity of the structure (*EM*), which is the effective property of the whole specimen and takes into account the effects of lattice arrangement, manufacturing defects, relative density and parent material. The second property was the Young's modulus of the parent material (*YM*), which reflects only the state of the material and manufacturing defects and is independent of lattice arrangement or relative density.

2.4. Porosity Evaluation

The process parameters used to additively manufacture the specimens should provide material with minimal porosity. However, in order to verify the quality of the fabrication, BFCCZ specimens were selected for porosity evaluation for two reasons. First, the BFCCZ specimens have the smallest strut diameters at given relative densities and as porosity increases with decreasing strut diameter,[21,28] porosity should be the worst for these specimens. Second, the BFCCZ specimens contain struts at all build angles, which also affects the porosity of the material.[29]

The BFCCZ specimens were metallographically processed and imaged using a Keyence VHX-6000 digital microscope (Keyence, Mechelen, Belgium). The images were then converted into binary monochrome images and the percentage of black area in the sample section (representing porosity) was analyzed using ImageJ software. The evaluation was carried out separately for the struts in each build angle.

2.5. Finite Element Analyses

Finite element analyses were performed using ANSYS Workbench (Ansys Inc., Canonsburg, Pennsylvania). The compression tests in the linear domain were simulated by two types of analyses using the nominal and parametric material model, which are described in Section 2.5.1.

2.5.1. Model of Material

The material AlSi10Mg was defined as a linear elastic material in ANSYS Workbench. For the nominal material model, the *YM* was set to 68.5 GPa, the Poisson's ratio to 0.33, and the density to 2670 kg m^{-3}.

To determine the actual mechanical properties of the parent material, the parametric material model was created using the *YM* of the parent material as a parameter. This procedure was based on the work of several authors who have shown that the real *YM* value is different for solid material and lattice structure.[28,47,48] The *YM* value was changed until the finite element analysis (FEA) results matched the experiment—the maximum deviation of the *EM* was set to 0.5 GPa. The other material properties remained unchanged.

2.5.2. Analysis Setup

Due to the simplicity of the calculation and stability, quarter models of lattice specimens were used—the symmetry constraints ensure the position of the specimen in the center and prevent the specimen from moving in the direction perpendicular to the loading direction. Two planes were added to the specimen to represent the loading surfaces of the testing machine (one fixed and one moving plane), which also prevent the specimen from moving in the direction parallel to the loading direction.

The thickness of the loading planes was set to 0.3 mm, and they were assigned the standard structural steel material with a *YM* 1000 times higher. This approach was used to simulate the several times higher stiffness of the testing machine compared to the lattice specimen. Both planes were meshed with Quad4 (Shell181) elements with a size of 1 mm (not the object of the simulation). The lattice specimens (material AlSi10Mg) were meshed with Tet10 (Solid187) elements with adaptive meshing. For element size selection, a mesh sensitivity analysis was performed on the specimen with the thinnest struts (BFCCZ with diameter of 1.95 mm) and the parameters monitored were the force response and the number of degrees of freedom (DOF). The resulting element size was set to 0.6 mm as it represents a compromise between accuracy (further refinement of the mesh leads to a change in force response of less than 5%—see **Figure 3**a) and computational effort (see Figure 3b).

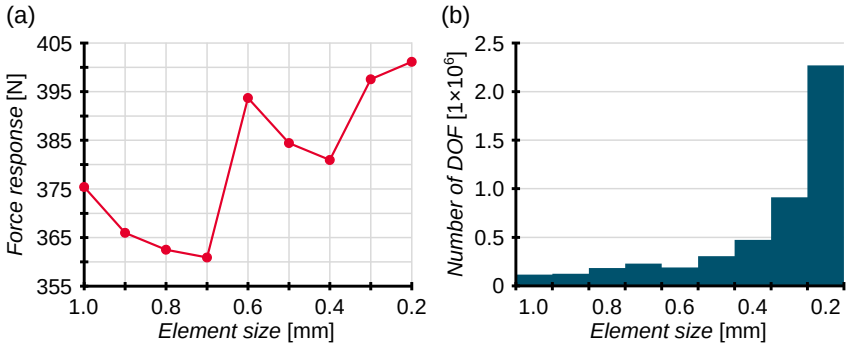

Figure 3. Effect of mesh refinement on a) change in force response and b) number of DOF.

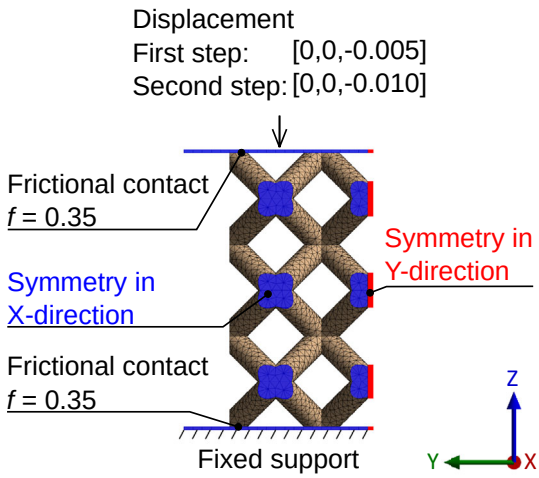

Figure 4. Boundary conditions of the FEA for the first group.

The bottom plane was fixed in displacement and rotation and a displacement condition was prescribed on the top plane (representing the actual test conditions). A two-step displacement of 0.01 mm (to ensure the linear elasticity region) in the *Z*- (first group) or *Y*- (second group) direction was used. The other degrees of freedom were restricted. The contacts between the specimen and the loading planes were specified as frictional with a friction coefficient *f* of 0.35 (table value for aluminum–steel contact).[49] An overview of the FEA setup can be found in **Figure 4**.

From the simulations, the force reactions in the loading surfaces were determined in the first step (displacement of 0.005 mm) and in the second step (displacement of 0.01 mm). The FEA results were processed using Equation (1)–(3) in the same way as the results of the mechanical tests.

3. Results and Discussion

3.1. FEA Results with Nominal Material Model

The graph in **Figure 5** shows the *EM* of the respective specimens using the FEA with nominal *YM* for the compression test in the *Z*-direction (Figure 5a) and *XY*-direction (Figure 5b). The difference in the maximum values for these two directions is ≈6.5 GPa (38.1 GPa and 31.6 GPa for FCCZ-0.7). The highest *EM* in both directions and for the entire range of relative densities was achieved by FCCZ, which is consistent with the literature.[34,50]

In the first group (*Z*-direction, Figure 5a), the highest resulting *EM* belong to the *Z*-variants of the lattice types. This is obviously due to the *Z*-struts, which are coaxial to the loading direction, as other authors have also noted.[32,44] Nevertheless, the FCC is stiffer in the *Z*-direction than BCCZ and BFCCZ, despite the absence of *Z*-struts. The reason for this is the different angle of the struts in FCC and BCC. In addition, the BFCC consists of more struts than the FCC and therefore the strut diameter must be smaller for a constant value of the relative density.

In the second group (*XY*-direction, Figure 5b), the *Z*-struts do not play a significant role and the *EM* of the basic variants and the variants with the *Z*-struts are quite similar. The results are mostly sorted by lattice topology, with FCC and FCCZ having the highest *EM* values, BFCC and BFCCZ in the middle, and BCC and BCCZ at the bottom.

The graphs in Figure 5 show that a significant difference in weight can be achieved at a constant *EM* value simply by changing the lattice topology. The largest difference is in the *Z*-direction for BCC with a relative density of 0.55 and FCCZ with a relative density of about 0.31. For the *XY*-direction, it is BCCZ with a relative density of 0.55 and FCCZ with a relative density of 0.39. It can be concluded that according to the FEA results, the mass saving by changing the lattice topology is up to 43% in the *Z*-direction and 29% in the *XY*-direction. The FEA thus confirms the first hypothesis in the *Z*-direction, but in the *XY*-direction there is a deviation of 1% (29% compared to the expected 30%).

Figure 6 shows the ratio of *EM* of the respective load directions. The BCC type is geometrically isotropic, so there is no difference between the load in the *XY*- and *Z*-direction. The BFCC type is the only one that is stiffer in the *XY*-direction than in the *Z*-direction, although the arrangement of the struts should have an opposite effect. In the BFCCZ type, the advantageous direction changes with the relative density. This change occurs at a relative density of 0.55. For all other specimens, loading in

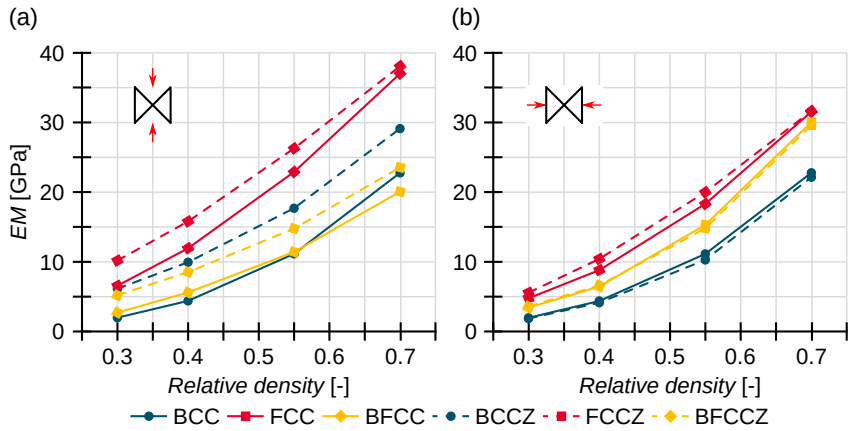

Figure 5. Results of FEA for loading in a) *Z*-direction and b) *XY*-direction.

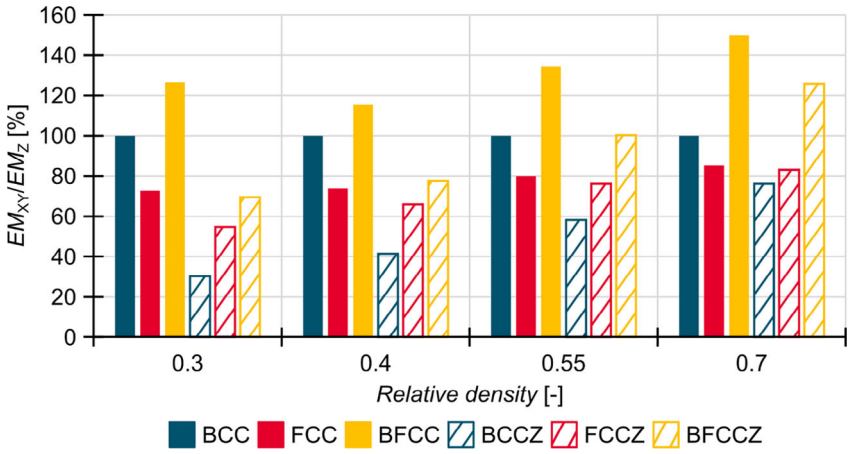

Figure 6. Ratio of *EM* for loading in *Z*- and *XY*-direction according to the FEA.

the *Z*-direction is more favorable for stiffness. Therefore, the second hypothesis is not generally confirmed by the FEA.

3.2. Experimental Testing

The graphs in **Figure 7** show the results of the experimental test in the *Z*-direction (Figure 7a) and *XY*-direction (Figure 7b). The first difference between the FEA and experimental results is the range of *EM* values obtained. The difference ranges from −18% for FCC-0.7 in the *Z*-direction to −72% for BCCZ-0.3 in the *Z*-direction. This is likely to be due to the decrease in mechanical properties (especially *YM*) of the parent material or a general defect caused by manufacturing or postprocessing. The second difference is the change in the ranking of lattice topologies in the *Z*-direction, with FCC being the stiffest at relative densities above 0.3 according to the experimental tests.

The average decrease in *EM* in the *Z*-direction is −47%. For all FCC samples, the decrease in *EM* was less than the average value (from −18% for FCC-0.7 to −45% for FCC-0.3). The *EM* of the other five lattice topologies decreased more than average at lower relative densities, but the *EM* decrease of the specimens with higher relative densities was less than average. The highest decrease was achieved by the FCCZ and BFCCZ specimens. All specimens with a relative density of 0.7 show the lowest decrease in *EM*. This indicates a decrease in stiffness for smaller diameter struts, which has also been reported by other authors.[28,47,48]

On the other hand, Figure 7b, which presents the results of the experimental test in the *XY*-direction, shows the same ranking as in the case of the FEA. The decrease in *EM* is also lower, namely, −34% on average. Unfortunately, the specimen BFCCZ-0.7 clearly deviates from the normal behavior. At a relative density of 0.7, an even lower *EM* is achieved than at a relative density of 0.55. This could be due to a local manufacturing error.

3.3. FEA Results with Parametric Material Model

As mentioned in Section 3.2, the experimentally determined *EM* values of the specimens were unexpectedly low, which most likely indicates changes in the parent material. Therefore, the parametric numerical study was performed to determine the true *YM* of the material for each specimen (details in Section 2.5.1). The FEA simulations were carried out until the numerically determined *EM* matched the experimentally determined (tolerance of 0.5 GPa was used).

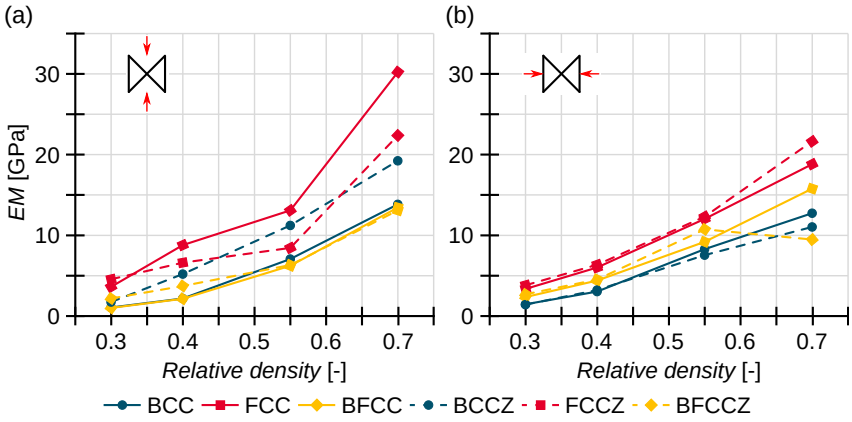

Figure 7. Results of experimental testing in a) *Z*-direction and b) *XY*-direction.

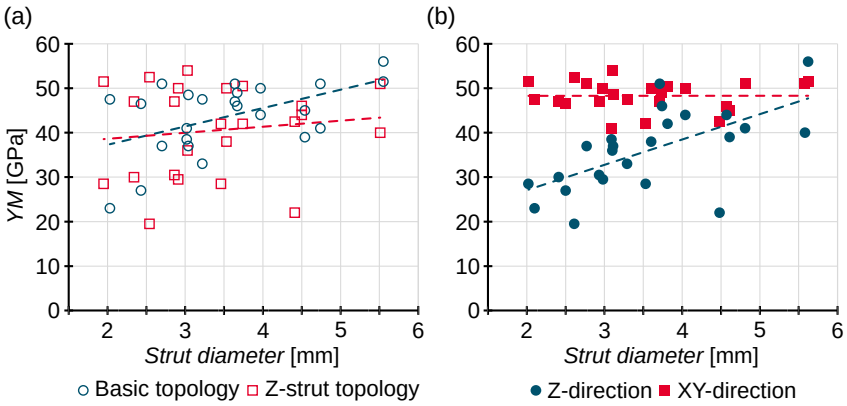

Figure 8. Final value of *YM* in parametric material model of all 46 tested specimens with linear trends and sorted by a) lattice topology and b) loading direction.

Figure 8 shows the relationship between the strut diameter and the resulting *YM* of the parametric material model. Figure 8a shows no correlation between the *YM* and the topology of the specimen, i.e., the presence of additional *Z*-struts has no influence on the observed major decrease of *EM*. However, when the legend of the graph is sorted according to the loading direction, as shown in Figure 8b, a strong dependency is clearly visible. The *YM* for the specimens loaded in the *XY*-direction is in the range of 41–54 GPa and decreases slightly with increasing strut diameter. On the other hand, the specimens loaded in the *Z*-direction show a significantly low *YM* with 17 out of 24 values below or equal to 40 GPa. The *YM* value increases with increasing strut diameter. The only exception is the specimen FCCZ-0.55 with a *YM* of only 22 GPa at a strut diameter of 4.41 mm and FCCZ-0.7 with a *YM* of 40 GPa and a strut diameter of 5.51 mm. This could also be a local manufacturing defects.

These results indicate a material anisotropy that has never been observed in additively manufactured AlSi10Mg material, especially after heat treatment. The possible cause is discussed in the following Section 3.4.

3.4. The Anisotropy of the Material

Authors who have studied the additively manufactured AlSi10Mg material agree that, with the exception of ductility, the material is not prone to anisotropy, which is commonly observed in additive manufacturing thanks to layer-by-layer fabrication.[9] Furthermore, the 6 h solution treatment used should completely eliminate the influence of the layers and homogenize the material.[45,46]

The specimens were randomly divided into two groups for the tests so that any influence of the fabrication, i.e., recoating problems, the flow of the protective atmosphere, the position on the platform with respect to the laser, or the position in the furnace, should have been minimized and is very unlikely.

The condition of the material in terms of porosity could be a valid reason. According to the metallographic samples, the small-diameter *Z*-struts at the edges of the specimens had higher porosity values (average of 0.58%) than the other struts (average of 0.28%) (see **Figure 9**). Therefore, their load-bearing capacity

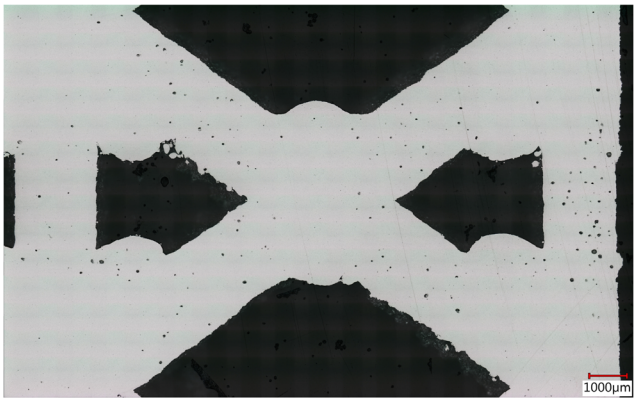

Figure 9. Metallographic sample of the BFCCZ specimen. The porosity of the *Z*-strut at the edge of the specimen is visibly higher than in the rest of the specimen.

was lower. This was more significant for loading in the *Z*-direction, as the *Z*-struts did not significantly affect the performance of the specimens when loaded in the *XY*-direction (Figure 5b and 7b). However, Figure 8a shows that the anisotropy is present regardless of the *Z*-strut. Moreover, even if the porosity of 0.6% was present in the entire specimen, the change in *YM* would be minimal (≈1.8% if the simple power law with a power of 3 is used for *YM* interpolation, which is included in the density-based topology optimization).[51] A more general explanation must therefore be found.

The next possible explanation is the accuracy of fabrication and the deformed shape of the struts due to the partially melted powder on the downskin of the struts, as reported by other authors.[28,47] **Figure 10**a, showing the BCC-0.3 specimen, shows a partially melted powder on the downskin of the struts. However, Figure 10b, which shows the vertical cross section of the strut of the same specimen, indicates that the downward-facing surface contains partially melted powder particles, but the shape is still circular. Furthermore, the typical elliptical shape with the major axis parallel to the *Z*-direction should increase the stiffness in the *Z*-direction, not otherwise. Finally, the authors report the significant deviations in strut shape for thinner struts.

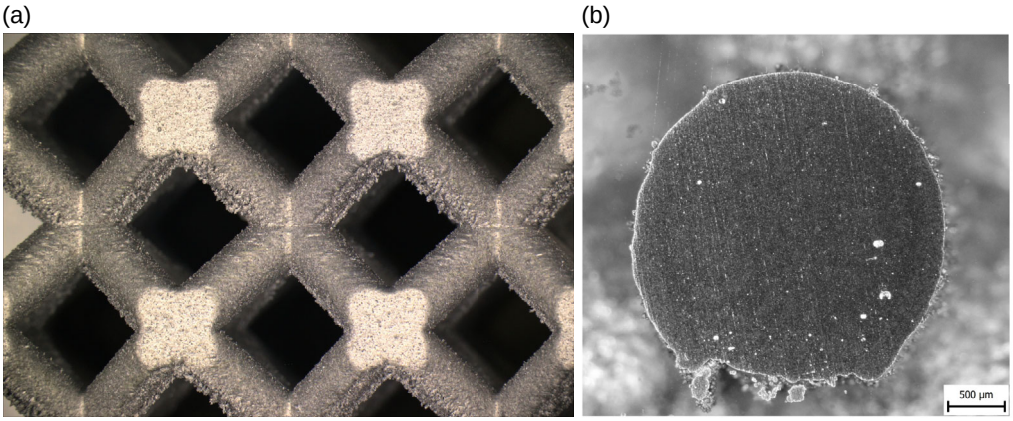

Figure 10. BCC0.3 specimen a) front view and b) cross section of a strut.

The diameters used in this study are usually reported to be free of significant defects.[21,28]

The last possible explanation is the presence of internal stresses in the material caused by water cooling during the T6 treatment. As Vaverka et al. have shown, the internal stress is always present and directional,[14] i.e., the water cooling has caused a preload in each sample that is directed toward the build platform. Assuming that the preload is constant across the platform, it should be more noticeable in the specimens with smaller strut diameters and especially affect the performance in the *Z*-direction. As the strut diameter increases, the effect should decrease and the loading in the *Z*- and *XY*-direction should become similar, as can be seen in Figure 8b for a strut diameter greater than ≈3.5 mm.

3.5. Experimental Comparison of Mechanical Performance of Lattice Types

In topology optimization, the required stiffness in a given region is defined by the reduced *YM* of the solid material (in this study, the *EM* of the structure is the same property) and is expressed by the value of the relative density calculated by some of the material interpolation schemes.[51] This comparative study shows that the choice of lattice topology is a crucial factor for the geometric representation of the topology optimization results. The best results in terms of stiffness and uniaxial compressive loading should be obtained with the FCCZ topology.

The experimental tests (Figure 7) show that up to 36% mass can be saved when loading in the *Z*-direction—the *EM* of the BFCC with a relative density of 0.55 is equal to the *EM* of the FCC at a relative density of about 0.35. In the *XY*-direction, the mass saving is 22% when the *EM* of BCCZ at a relative density of 0.55 is the same as that of FCCZ at a relative density of 0.43. The specimen BFCCZ-0.7 was excluded from the comparison. These results again confirm the first hypothesis for the *Z*-direction, but not for the *XY*-direction.

Figure 11 shows the ratio of *EM* for the *XY*- and *Z*-directions from experimental tests, which was influenced by the observed load dependence. Only 13/24 specimens show higher or at least equal *EM* values when loaded in the *Z*-direction, which is in contrast to the FEA results with 19/24 specimens. The BCC specimens are also anisotropic in the experiments. On the other hand, the experimental tests confirmed the numerical results that the BFCC type is more suitable for loading in the *XY*-direction for the whole range of relative densities.

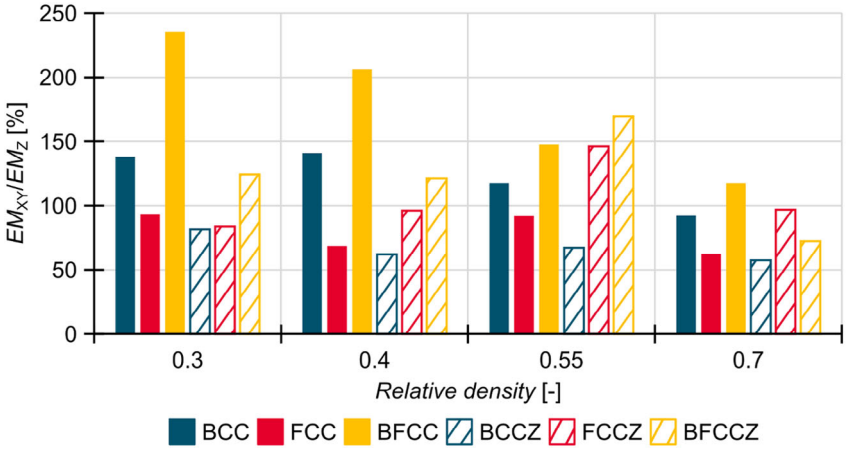

Figure 11. Ratio of *EM* for loading in *Z*- and *XY*-direction according to the experimental testing.

Therefore, the second hypothesis could not be generally confirmed and is limited to the FCC and BCCZ lattice types.

In the extreme case where the part consists of a BCCZ lattice structure with a relative density of 0.55 and is loaded in the *XY*-direction, the resulting *EM* of the structured material is ≈10 GPa (FEA) or 7.5 GPa (experiment). Then, by changing the lattice topology, in this case FCCZ (FEA) or FCC (experiment) and changing the manufacturing orientation to change the load direction to *Z*-direction, the resulting relative density is ≈0.3 (FEA) or ≈0.37 (experiment) with the same *EM* value. This means a mass saving of 44.5% (FEA) or 32.7% (experiment) with the same stiffness of the structure.

3.6. Material Model for Topology Optimization

The motivation for the numerical and experimental comparison of the elastic properties of aluminum truss-based lattice structures was their potential use in multiscale topology optimization. However, the experimental tests showed an unexpected anisotropic behavior, so that the deviation between the experimental and numerical results was large. From this fact, two suggestions for use in multiscale topology optimization can be derived: 1) The material interpolation model in density-based multiscale topology optimization using an arbitrary truss-based lattice structure made of AlSi10Mg material in the T6 state must account for the observed anisotropy and cannot be isotropic. At the very least, different material models should be used for elements loaded in the direction perpendicular and parallel to the build direction; and 2) The value of *YM* of truss-based lattice structures should take into account the effect of residual stresses on the resulting EM of the structure under different loading conditions.

To prepare a specific material interpolation model for the multiscale topology optimization, an empirical equation for AlSi10Mg in the T6 state is proposed. Equation (4) represents the estimation of *YM* (in GPa) as a function of the strut diameter *D* (in mm) when the loading is parallel to the build direction. For perpendicular loading, the equation is not required, as no correlation was observed and *YM* remained constant

$$YM\,[\mathrm{GPa}] = 5.7\,D\,[\mathrm{mm}] + 16.1 \tag{4}$$

The validity of the Equation (4) was tested on six additional specimens (one for each lattice topology) with different strut diameters in the previously tested area and the values of their *EM* should be similar. All specimens were subjected to the compression test parallel to the build direction. The experimental results are shown in **Table 2** in comparison to the numerical results with two different material models. The first one is the nominal material model with constant *YM* (as described in Section 2.5.1.) and the second material model uses Equation (4) to estimate the *YM* for the structure. When the proposed Equation (4) is used, the improved accuracy of the numerical calculation is clearly visible.

Table 2. The comparison of experimental data and two numerical results for six additional specimens.

Specimen	Strut diameter [mm]	*EM* (experiment) [GPa]	Error of *EM* (FEA with nominal material as described in Section 2.5.1) [%]	Error of *EM* (FEA with Equation (4)) [%]
BCC	4.26	7.32	+108	+23
FCC	3.90	7.59	+100	+12
BFCC	3.43	8.33	+130	+20
BCCZ	3.54	8.31	+83	−3
FCCZ	3.40	7.67	+99	+3
BFCCZ	3.04	6.10	+174	+34

4. Conclusion

This work dealt with the experimental and numerical evaluation of structured materials for use in multiscale topology optimization. The aim was to compare different lattice types and to test two hypotheses, namely, that a significant saving of mass while maintaining stiffness is possible when changing the lattice topology for the geometric representation of the optimization results or when changing the fabrication orientation and thus the loading direction of an optimized part. Six truss-based lattice types with a relative density in the range of 0.3–0.7 were included in the study. The lattice topologies were subjected to FEA and evaluated in two uniaxial loading directions. The lattice topologies were fabricated from AlSi10Mg material using LPBF technology and heat treated to T6 condition for experimental comparison. The specimens were then subjected to compressive loading in the direction parallel to the build direction (*Z*-) and perpendicular to it (*XY*-).

The conclusions of this article can be summarized in points: 1) The first hypothesis was confirmed for the *Z*-direction by FEA and by the experiments. The mass saving caused by the change of the lattice topology could reach up to 43% (FEA) or 36% (experiment). In the *XY*-direction, the mass saving was less than 30% (29% and 22%, respectively); 2) The second hypothesis could not be generally confirmed and is only limited to the FCC and BCCZ lattice types. For the other lattice types, the direction parallel to the build direction is not generally advantageous and depends on the relative density or is even generally not advantageous (BFCC topology); 3) If both hypotheses are combined, the mass saving with constant stiffness is 44.5% (FEA) or 32.7% (experiment); 4) In both loading directions, the FCC or FCCZ topologies achieved the highest values of the effective modulus of elasticity. On the other hand, the lowest values were obtained for the BCC topology; and 5) The experiments showed a significant anisotropic behavior of the specimens, independent of the lattice topology. The authors suggest that the anisotropy is caused by the inner stress induced by the water cooling during the T6 treatment and proposed material model for variable Young's modulus for loading in *XY*-direction.

The superiority of the FCC and FCCZ topologies has only been demonstrated for compressive loading. However, the real parts are rarely loaded in pure compression. Therefore, future work should focus on the comparison of the lattice topologies in shear, torsion, and especially in mixed loading. Such a complex comparison is necessary to prove the suitability of the respective lattice topologies for real loading conditions.

Acknowledgements

This article presents results of the research that has received funding from the faculty specific research project FSI-S-23-8340 and "Mechanical Engineering of Biological and Bio-inspired Systems", funded as project no. CZ.02.01.01/00/22_008/0004634 by Programme Johannes Amos Commenius, call Excellent Research.

Open access publishing facilitated by Vysoke uceni technicke v Brne, as part of the Wiley - CzechELib agreement.

Conflict of Interest

The authors declare no conflict of interest.

Data Availability Statement

The data that support the findings of this study are openly available in [Zenodo.org] at [10.5281/zenodo.10513025], reference number [10513025].

Keywords

aluminum alloys, compression tests, effective modulus of elasticity, heat treatment, laser powder bed fusion

Received: January 18, 2024
Revised: April 15, 2024
Published online: May 28, 2024

[1] M. P. Bendsøe, N. Kikuchi, *Comput. Methods Appl. Mech. Eng.* **1988**, *71*, 197.
[2] J. Wu, O. Sigmund, J. P. Groen, *Struct. Multidiscip. Optim.* **2021**, *63*, 1455.
[3] H. Rodrigues, J. M. Guedes, M. P. Bendsoe, *Struct. Multidiscip. Optim.* **2002**, *24*, 1.
[4] D. Brackett, I. Ashcroft, R. Hague, in *22nd Annual Int. Solid Freeform Fabrication Symp.*, University of Texas at Austin, Austin, United States **2011**, p. 348.
[5] L. J. Gibson, M. F. Ashby, in *Cellular Solids: Structure and Properties*, Cambridge University Press, Cambridge **1997**.
[6] O. Vaverka, D. Koutny, D. Palousek, *Rapid Prototyping J.* **2019**, *25*, 1545.
[7] M. Orme, I. Madera, M. Gschweitl, M. Ferrari, *Designs* **2018**, *2*, 51.
[8] K. Kempen, L. Thijs, J. Van Humbeeck, J.-P. Kruth, *Phys. Proc.* **2012**, *39*, 439.
[9] T. Maconachie, M. Leary, J. Zhang, A. Medvedev, A. Sarker, D. Ruan, G. Lu, O. Faruque, M. Brandt, *Mater. Sci. Eng. A* **2020**, *788*, 139445.
[10] J. Fiocchi, A. Tuissi, C. A. Biffi, *Mater. Des.* **2021**, *204*, 109651.
[11] N. T. Aboulkhair, I. Maskery, C. Tuck, I. Ashcroft, N. M. Everitt, *Mater. Sci. Eng. A* **2016**, *667*, 139.
[12] A. Mertens, O. Dedry, D. Reuter, O. Rigo, J. Lecomte-Beckers, in *Proc. of the 26th Int. Solid Free Form Fabrication (SFF) Symp.*, University of Texas at Austin, Austin, United States **2015**, p. 1007.
[13] A. Suzuki, K. Sekizawa, M. Liu, N. Takata, M. Kobashi, *Adv. Eng. Mater.* **2019**, *21*, 1900571.
[14] O. Vaverka, D. Koutný, R. Vrána, L. Pantělejev, D. Paloušek, in *Engineering Mechanics 2018*, Institute of Theoretical and Applied Mechanics of the Czech Academy of Sciences, Praha **2018**, p. 897.
[15] S. Megahed, J. Bühring, T. Duffe, A. Bach, K.-U. Schröder, J. H. Schleifenbaum, *Metals* **2022**, *12*, 1311.
[16] I. Maskery, N. T. Aboulkhair, A. O. Aremu, C. J. Tuck, I. A. Ashcroft, R. D. Wildman, R. J. M. Hague, *Mater. Sci. Eng. A* **2016**, *670*, 264.
[17] X. Wang, R. Qin, X. Zhang, B. Chen, *Thin-Walled Struct.* **2023**, *183*, 110434.
[18] J. Fiocchi, C. Bregoli, G. Gerosa, A. Tuissi, C. A. Biffi, *Adv. Eng. Mater.* **2021**, *23*, 2100418.
[19] E. Ossola, A. A. Shapiro, A. Pate, S. Firdosy, E. Brusa, R. Sesana, *Proc. Inst. Mech. Eng., Part L* **2021**, *235*, 2071.
[20] M. Sos, G. Meyer, K. Durst, C. Mittelstedt, E. Bruder, *Mater. Des.* **2023**, *227*, 111796.
[21] R. Vrána, J. Jaroš, D. Koutný, J. Nosek, T. Zikmund, J. Kaiser, D. Paloušek, *J. Manuf. Process.* **2022**, *74*, 640.
[22] U. Gebhardt, T. Gustmann, L. Giebeler, F. Hirsch, J. K. Hufenbach, M. Kästner, *Mater. Des.* **2022**, *220*, 110796.
[23] H. Lei, C. Li, X. Zhang, P. Wang, H. Zhou, Z. Zhao, D. Fang, *Addit. Manuf.* **2021**, *37*, 101674.
[24] T. Maconachie, M. Leary, P. Tran, J. Harris, Q. Liu, G. Lu, D. Ruan, O. Faruque, M. Brandt, *Int. J. Adv. Manuf. Technol.* **2022**, *118*, 4085.
[25] T. Yu, H. Hyer, Y. Sohn, Y. Bai, D. Wu, *Mater. Des.* **2019**, *182*, 108062.
[26] A. T. Erturk, M. E. Bulduk, G. Tarakçi, G. Özer, E. Yarar, *Met. Mater. Int.* **2022**, *28*, 155.
[27] A. Villuendas, J. Jorba, A. Roca, *Metall. Mater. Trans. A* **2014**, *45*, 3857.
[28] Z. Dong, X. Zhang, W. Shi, H. Zhou, H. Lei, J. Liang, *Materials* **2018**, *11*, 2463.
[29] Z. Dong, Y. Liu, W. Li, J. Liang, *J. Alloys Compd.* **2019**, *791*, 490.
[30] M. Leary, M. Mazur, J. Elambasseril, M. McMillan, T. Chirent, Y. Sun, M. Qian, M. Easton, M. Brandt, *Mater. Des.* **2016**, *98*, 344.
[31] H. Alsalla, L. Hao, C. Smith, *Mater. Sci. Eng. A* **2016**, *669*, 1.
[32] P. Hanzl, I. Zetkova, M. Dana, in *DAAAM Proc.* (Ed: B. Katalinic), DAAAM International, Vienna **2017**, p. 0481.
[33] R. Wauthle, B. Vrancken, B. Beynaerts, K. Jorissen, J. Schrooten, J.-P. Kruth, J. Van Humbeeck, *Addit. Manuf.* **2015**, *5*, 77.
[34] A. Aremu, I. Maskery, C. Tuck, I. Ashcroft, R. Wildman, R. Hague, in *Proc. of the 25th Int. Solid Free Form Fabrication (SFF) Symp.*, University of Texas at Austin, Austin, United States **2014**, p. 1238.
[35] M. Fernández, F. Fritzen, O. Weeger, *Int. J. Numer. Methods Eng.* **2022**, *123*, 577.
[36] J. Wang, A. Panesar, *Addit. Manuf.* **2022**, *60*, 103238.
[37] D. Kang, S. Park, Y. Son, S. Yeon, S. H. Kim, I. Kim, *Mater. Des.* **2019**, *175*, 107786.
[38] C. Wang, X. Gu, J. Zhu, H. Zhou, S. Li, W. Zhang, *Struct. Multidiscip. Optim.* **2020**, *61*, 869.
[39] X. Liu, L. Gao, M. Xiao, *Comput. Methods Appl. Mech. Eng.* **2023**, *415*, 116209.
[40] Z. Du, X.-Y. Zhou, R. Picelli, H. A. Kim, *J. Mech. Des.* **2018**, *140*, 111417.
[41] S. Zhou, Q. Li, *J. Mater. Sci.* **2008**, *43*, 5157.
[42] E. Garner, H. M. A. Kolken, C. C. L. Wang, A. A. Zadpoor, J. Wu, *Addit. Manuf.* **2019**, *26*, 65.
[43] M. F. Ashby, *Philos. Trans. R. Soc., A* **2006**, *364*, 15.
[44] M. Smith, Z. Guan, W. J. Cantwell, *Int. J. Mech. Sci* **2013**, *67*, 28.
[45] P. Delroisse, P. J. Jacques, E. Maire, O. Rigo, A. Simar, *Scr. Mater.* **2017**, *141*, 32.
[46] M. Liu, N. Takata, A. Suzuki, M. Kobashi, *Materials* **2020**, *13*, 2487.
[47] O. Červinek, B. Werner, D. Koutný, O. Vaverka, L. Pantělejev, D. Paloušek, *Materials* **2021**, *14*, 2462.
[48] S. Tsopanos, R. A. W. Mines, S. McKown, Y. Shen, W. J. Cantwell, W. Brooks, C. J. Sutcliffe, *J. Manuf. Sci. Eng.* **2010**, *132*, 041011.
[49] P. J. Blau, in *ASM Handbook, Volume 18 – Friction, Lubrication and Wear Technology*, ASM International, Materials Park **1992**.
[50] M. Mazur, M. Leary, S. Sun, M. Vcelka, D. Shidid, M. Brandt, *Int. J. Adv. Manuf. Technol.* **2015**, *84*, 1391.
[51] M. P. Bendsøe, O. Sigmund, *Arch. Appl. Mech.* **1999**, *69*, 635.